Ordering, Martensitic and Ferromagnetic Transformations in Ni-Al-Mn Heusler Shape Memory Alloys

Materials Transactions, JIM, Vol. 41, No. 8 (2000) pp. 943 to 949
Special Issue on Effect of Magnetic Field on Phase Transformations and Essential Physical Properties of Materials

Ordering, Martensitic and Ferromagnetic Transformations in Ni–Al–Mn Heusler Shape Memory Alloys

Ryosuke Kainuma[1], Fumihiko Gejima[1,*], Yuji Sutou[1,*], Ikuo Ohnuma[1] and Kiyohito Ishida[2]

[1]*Department of Materials Science, Graduate School of Engineering, Tohoku University, Sendai 980-8579, Japan*
[2]*New Industry Creation Hatchery Center (NICHe), Tohoku University, Sendai 980-8579, Japan*

Order-disorder, martensitic and magnetic transformations in the Ni_2AlMn alloys have been investigated by differential scanning calorimetry (DSC), X-ray diffraction (XRD) and transmission electron microscopy (TEM) techniques. The critical temperatures corresponding to the above transformations have been determined. It is shown that, on aging at low temperature, the parent phase structure changes from that of B2 to $L2_1$ by an ordering reaction causing the *Ms* temperature to decrease. The Curie temperature which has the highest value of about $T_c = 92°C$ at the Ni_2AlMn composition decreases steeply on deviating from the stoichiometric composition. Two kinds of new martensite phases have also been detected in the as-aged Ni–21Al–25Mn and Ni–22Al–25Mn alloys.

(Received March 16, 2000; Accepted May 8, 2000)

Keywords: *martensitic transformation, magnetic shape memory alloy, order-disorder transition, magnetic transition, Ni_2AlMn Heusler alloy*

1. Introduction

Recently, the present authors' group has investigated the phase equilibria and the stability of several phases in the Ni-rich portion of the Ni–Al–Mn ternary system,[1] and determined some characteristic features such as the *Ms* temperature, crystal structure of the martensite phases and the shape memory properties of the $\beta(B2)/\beta'$ (2M: $L1_0$) martensitic transformation.[2,3] Figure 1 shows the isothermal section diagram at 850°C and the iso-*Ms* temperature contour.[2] It is seen that the wide β single-phase region extends from the Ni–Al phase to the Ni–Mn intermetallic phase, and the alloys with compositions in the vicinity of Ni–Mn have a very high *Ms* temperature. It has also been reported that the Ni–Al–Mn β base alloys with a small amount of $\gamma(A1)$ phase show some ductility and shape memory effect at elevated temperatures.[3] While the alloys quenched from elevated temperatures over 1000°C have the B2 structure and show a para/antiferro magnetic transition at about 20°C,[4] low temperature aging at 350 to 400°C after quench, induces parent phase ordering from the B2 structure to the $L2_1$ Heusler-type structure.[5] Very recently, the present authors have found that some of these $L2_1$ ordered alloys show both the para/ferro magnetic and the martensitic transformations.[6] Ullakko *et al.* have proposed that the ferromagnetic Ni_2GaMn shape memory (SM) alloys with the $L2_1$ structure have potential for use as a new type of smart material whose SM properties can be controlled not only by temperature and stress, but also by a magnetic field.[7] It is expected therefore, that such effects may be present in the related Ni–Al–Mn system of alloys, which also exhibit thermoelastic martensitic and magnetic transformations.

Although the correlation between ordering, martensitic and magnetic transitions have been reported mainly in some Fe base alloys, such as the Fe–Pt, Fe–Pd, Fe–Mn–Si and Fe–Ni base martensite alloys,[8] such correlation studies are very few in the non-ferrous alloy systems. The characteristic features of these transitions occurring in the Ni–Al–Mn alloys are likely to be interesting both from a practical and a theoretical phase-stability view point. It is the purpose of this paper to examine the effect of low temperature aging on the order-disorder, martensitic and magnetic transitions of the Ni–Al–Mn alloys and to clarify the correlation between ordering, martensitic and magnetic transitions in this system.

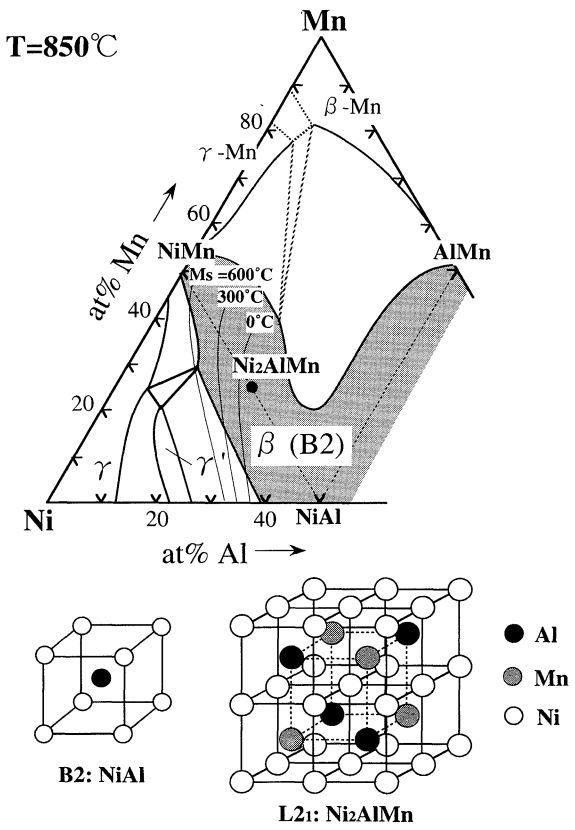

Fig. 1 Phase Diagram of the Ni–Al–Mn System at 850°C. The iso-*Ms* lines of martensitic transformation occurring in the B2 parent phase are indicated by thin lines.

*Graduate Students, Tohoku University.

2. Experimental Procedures

Ni–(12–27.5) at%Al–(15–38) at%Mn ternary alloys with the β single-phase structure were prepared in an induction furnace under an argon atmosphere by melting pure metals Ni (99.9%), Al (99.7%) and Mn (99.9%) in appropriate quantities. All the cast alloys were solution treated at 1000°C for 72 h and quenched into ice water. Some alloys were aged at 300 or 400°C to obtain an ordered $L2_1$ structure. All the transformation temperatures were determined by differential scanning calorimetric (DSC) measurements. Thin foils for TEM examination were prepared by jet-polishing sliced specimens from the alloys in a solution of 20% perchloric acid in methanol. Electron diffraction and transmission electron microscopic (TEM) observations were carried out using a JEM2000EX. TEM observations at low temperatures were carried out using a cold stage holder. X-ray diffraction (XRD) investigation on powder specimens using Cu–Kα radiation was conducted to identify and characterize the phases present. Low temperature XRD measurements were carried out using a Philips X'part system with provision for low temperature measurements.

3. Results and Discussion

3.1 Order-disorder transition

Previous studies have shown that the B2/$L2_1$ order-disorder transition temperature can be associated with the onset of an endothermic peak in the DSC heating curve for some alloys aged at 350 to 400°C.[5,6] All the data on the ordering temperatures (T_c^o) determined by such DSC measurements are listed in Table 1 and plotted in Fig. 2. It is seen that while the T_c^o temperatures are a function of both Mn and Al contents, the Al content has a more significant effect on the T_c^o temperatures. A thermodynamic analysis on the basis of the

Table 1 Critical temperatures of the chemical and magnetic ordering transitions.

Composition		T_c^o(B2/$L2_1$)	T_c^m(para/ferro)
at%Al	at%Mn	(°C)	(°C)
18	32	455	—
20	25	464	—
20	30	466	38
21	25	468	—
21.75	25	483	—
22	25	482	16
22	28	498	51
22.5	20	472	—
22.5	22.5	487	—
22.5	25	494	26
25	17.5	488	—
25	20	496	1
25	22.5	501	4
25	25	502	92
27.5	20	480	12
27.5	22.5	533	50
30	20	531	40

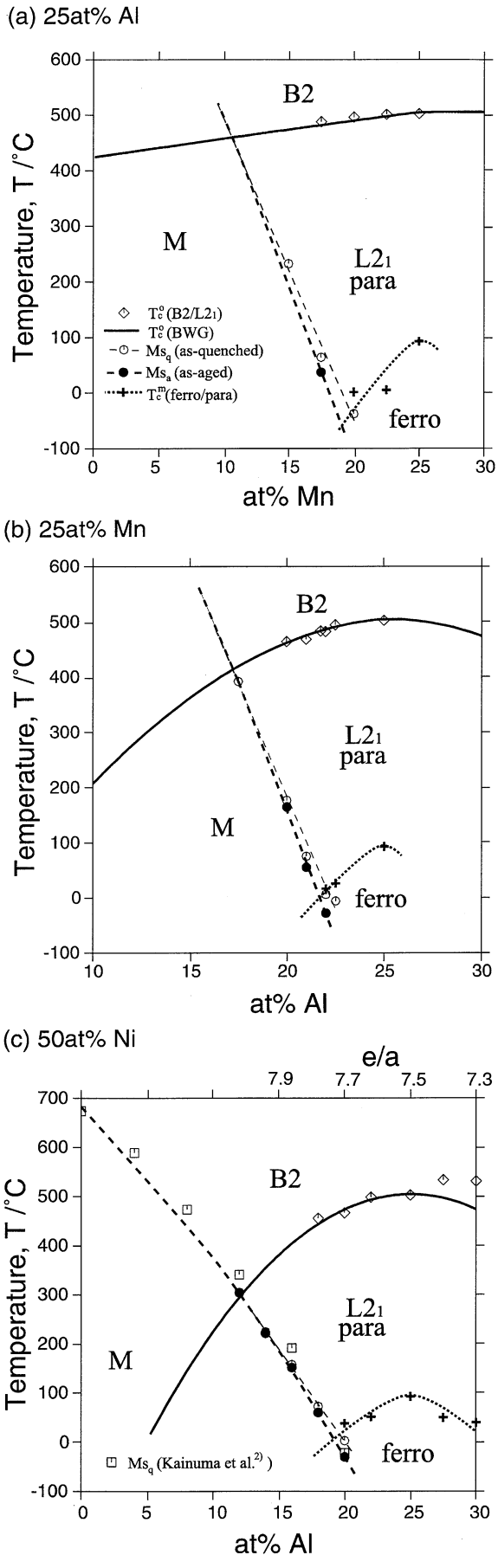

Fig. 2 Ordering, martensitic and magnetic transition temperatures of the aged (a) Ni–25Al–Mn, (b) Ni–Al–25Mn and (c) 50Ni–Al–Mn alloys determined by DSC measurement.

experimental results was performed in order to estimate the pair interchange energies between Ni, Al and Mn atoms.

3.1.1 Theoretical calculation model

The Bragg-Williams-Gorsky (BWG) model modified by Inden[9] was applied for the present thermodynamic analysis. The i-j pair interchange energies of the k'th nearest neighbors (n.n.) $W_{ij}^{(k)}$ are defined by $W_{ij}^{(k)} = -2V_{ij}^{(k)} + V_{ii}^{(k)} + V_{jj}^{(k)}$, where $V_{ii}^{(k)}$, $V_{jj}^{(k)}$ and $V_{ij}^{(k)}$ are the chemical bonding energies. A positive value for $W_{ij}^{(k)}$ implies a tendency to order and a negative value, a tendency to cluster. $W_{ij}^{(k)}$ values can be evaluated from the A2/B2 order-disorder transition temperature T_{cij}°(A2/B2) of the stoichiometric ordered-phase B2 by the following equation;

$$T_{cij}^{\circ}(\mathrm{A2/B2}) = (2W_{ij}^{(1)} - 1.5W_{ij}^{(2)})/k = E_{ij}/k, \quad (1)$$

where k is Boltzmann's constant.[9] Since the B2/D0$_3$ order-disorder transition temperature T_{cij}°(B2/D0$_3$) of the D0$_3$ alloys is also a function of both $W_{ij}^{(1)}$ and $W_{ij}^{(2)}$, the values of both $W_{ij}^{(1)}$ and $W_{ij}^{(2)}$ can be evaluated using the T_{cij}°(A2/B2) and T_{cij}°(B2/D0$_3$) values. It should be noted here that the interchange energy data extracted from the ordering temperatures using such a relation based on the BWG model are in general smaller in magnitude than those obtained with more precise models such as the cluster variation method (CVM).[10]

3.1.2 Estimate of interchange energies

The value of E_{MnAl} in eq. (1) was estimated from the experimental value of T_c° for the B2 phase in the Mn–Al system.[11] Since the D0$_3$ phase does not appear in the Mn–Al binary system, the value of $W_{\mathrm{MnAl}}^{(2)}$ was evaluated from the B2/L2$_1$ ordering temperatures measured in the Ni–Al–Mn system.

The direct estimation of the interchange energies for the Ni–Al pair was difficult because of the absence of a disordered bcc phase in the Ni–Al phase diagram. Recent investigations on the stability of the B2 phase in many Co–Al–X ternary systems had however shown that the A2–B2 transition temperatures in the CoAl–X section were located on a common straight line independent of the type of X element, starting from an original point at −273°C (0 K) in pure X (*i.e.* 100 at%X).[12] This was confirmed by a BWG calculation in one particular case where the interchange energy of one combination A–B was several times more positive than those of other combinations B–C and C–A.[1] On the basis of the assumption that such the characteristic feature is met in the Ni–Al–X ternary systems, the NiAl ordering temperature $T_{c\mathrm{NiAl}}^{\circ}$(A2/B2) (about 4230°C) was estimated by an extrapolation of the experimental ordering temperatures[13] in the Fe-rich portion to the AlNi axis in the AlNi–Fe pseudobinary system. The T_c° of the metastable B2/D0$_3$ transition in the Ni$_3$Al alloy was estimated by extrapolation from the present data obtained for the Ni$_{(2+x)}$AlMn$_{(1-x)}$ alloys as shown in Fig. 2(a).

Since the stable NiMn–B2 phase existed up to 911°C and the A2/B2 transition did not appear in the stable Ni–Mn binary phase diagram, $T_{c\mathrm{NiMn}}^{\circ}$(A2/B2) could not be directly evaluated. From the Ni–Al–Mn ternary phase diagram however it was taken that the $T_{c\mathrm{NiMn}}^{\circ}$(A2/B2) temperature could not be fairly higher than 911°C.[1] The value of $W_{\mathrm{NiMn}}^{(2)}$ was evaluated from the present B2/L2$_1$ ordering data in the Ni–Al–Mn system, since there was no direct information on the ordering temperature $T_{c\mathrm{NiMn}}^{\circ}$(B2/D0$_3$) in the Ni–Mn binary system. All the interchange energy values obtained in the present calculation are summarized in Table 2.

Table 2 Pair interchange energies used for BWG calculation.

Atom pair		$W_{XY}^{(1)}$ (k-unit)	$W_{XY}^{(2)}$ (k-unit)
X	Y		
Ni	Al	2600	465
Al	Mn	1014	519
Mn	Ni	600	0

3.1.3 Results of calculation

The B2/L2$_1$ boundary drawn as a thick line in Figs. 2(a) to (c) is from the results of present calculation. Calculated results are in fairly good agreement with all the experimental data. Figure 3 shows the iso-T_c° contour lines. The high T_c° line exists along the Ni$_3$Al–Ni$_2$AlMn section. Such a characteristic feature is to be attributed to the fact that the second nearest neighbour interchange energies $W_{\mathrm{NiAl}}^{(2)}$ and $W_{\mathrm{MnAl}}^{(2)}$ in the Ni–Al and Mn–Al systems are relatively larger than those of the Ni–Mn pair.

3.2 Martensitic transformations

3.2.1 *Ms* temperature

Figure 4 shows the effect of aging time on the *Ms* temperature in the Ni–22Al–25Mn alloy. It is seen that the *Ms* temperature in the as-quenched specimen decreases drastically from a value of $Ms_q = 6$°C at the beginning of aging to $Ms_a = -20$°C after about 10 min at 400°C and to about $Ms_a = -40$°C after about 30 min at 300°C, respectively. The change in the *Ms* temperature due to aging ($\Delta Ms = Ms_q - Ms_a$) depends on the aging temperature; the change ($\Delta Ms \approx 45$°C) in specimen aged at 300°C is larger than that ($\Delta Ms \approx 25$°C) observed in the specimen aged at 400°C. All

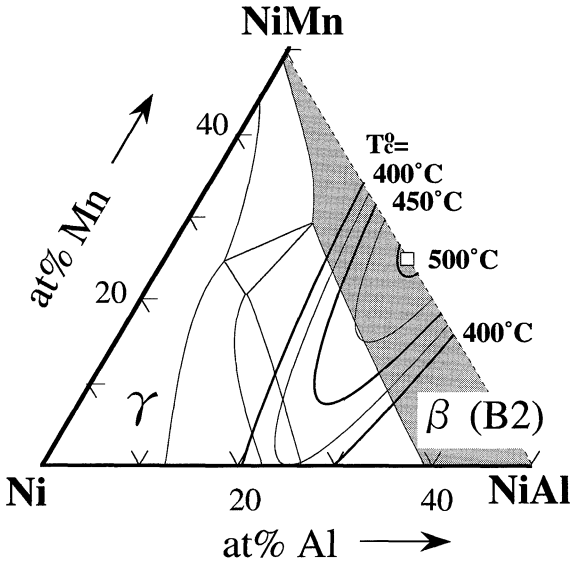

Fig. 3 The iso-T_c° contours obtained by the BWG calculation.

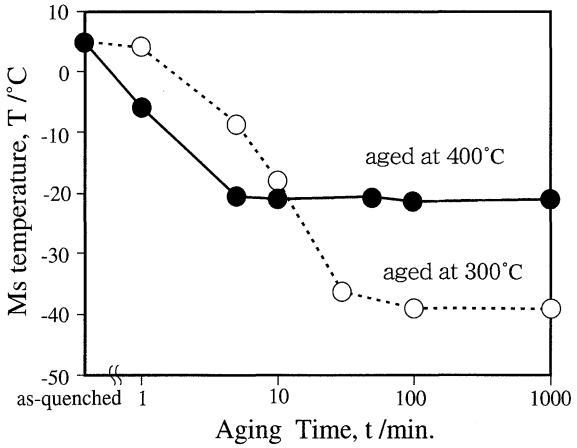

Fig. 4 *Ms* temperatures of the Ni–22Al–25Mn alloys vs aging time.

the *Ms* data on as-quenched and specimens aged at 400°C for 72 h are listed in Table 3 and plotted in Fig. 2. It is seen that ΔMs depends on the alloy composition and that the Ms_a of aged specimens are always lower than the Ms_q of as-quenched specimens of the same alloy. These facts suggest,

(i) the degree of *Ms* change due to aging is a function of the degree of equilibrium $L2_1$ long-range order reached at the aging temperature. The specimens aged at lower temperatures could be expected to have higher degree of order than those aged at higher temperatures,

(ii) the differences in the times needed for reaching the steady state equilibrium condition at 300°C and 400°C are to be attributed to the differences in the diffusivity of atoms at the different aging temperatures.

Figures 5(a) and (b) show the iso-Ms_a and iso-ΔMs contours, respectively, which are estimated from the data listed in Table 3. The iso-Ms_a contour lines are similar to the iso-Ms_q lines in the as-queched specimens as shown in Fig. 1.[2] It is interesting to note that the shape of the iso-ΔMs lines is

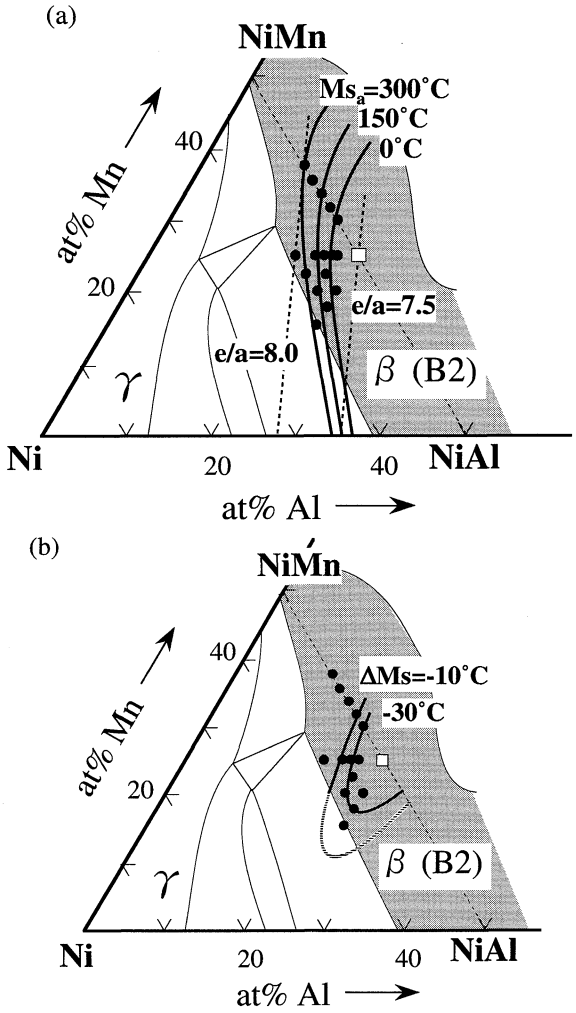

Fig. 5 The (a) iso-Ms_a and (b) iso-ΔMs contours.

Table 3 Martensitic transformation temperatures of specimens quenched and aged at 400°C for 72 h.

Specimen		As-quenched (°C)				As-aged (°C)				ΔMs (°C)
at%Al	at%Mn	Ms_q	Mf_q	As_q	Af_q	Ms_a	Mf_a	As_a	Af_a	
12	38	303	279	298	317	304	274	299	324	1
14	36	224	203	217	240	221	204	220	239	−3
16	34	157	109	123	168	151	89	108	164	−6
17.5	25	392	375	474	500	—	—	—	—	—
18	32	72	43	69	97	60	27	49	76	−12
20	22.5	315	291	404	422	—	—	—	—	—
20	25	176	151	167	196	164	108	123	179	−12
20	30	3	−23	−9	16	−30	−67	−61	−13	−33
21	25	75	43	64	90	55	18	36	71	−20
21.75	25	32	−6	22	52	12	−15	−1	28	−20
22	25	6	−27	−5	22	−28	−65	−27	−10	−34
22.5	20	205	167	275	329	177	159	167	190	−28
22.5	22.5	85	40	58	100	49	−21	9	64	−36
22.5	25	−6	—	—	—	—	—	—	—	—
25	15	233	206	449	472	—	—	—	—	—
25	17.5	64	33	58	84	37	2	23	59	−27
25	20	−38	—	—	−21	—	—	—	—	—

very similar to those of the iso-T_c^o lines obtained by the BWG calculation shown in Fig. 3. This fact supports the explanation for the aging effect, namely that the degree of *Ms* change due to aging is a function of the equilibrium degree of $L2_1$ order. It is also concluded that the B2 to $L2_1$ ordering stabilizes the parent phase rather than the martensite phase. The effect of the para/ferro magnetic transition on the *Ms* temperature is not very obvious and may not be significant as can be seen from Fig. 2.

3.2.2 Crystal structure of martensite phases

Previous studies[2,14] had revealed that the B2 parent phase in the Ni–Al–Mn alloys transforms martensitically to yield product phases with different stacking sequences. The product phases found are the 2M phase with the stacking sequence $(1)_2$, the 10M phase with the stacking sequence $(3\bar{2})_2$, the 12M phase with the stacking sequence $(5\bar{2}3\bar{2})$ or/and the 14M phase with the stacking sequence $(5\bar{2})_2$. The 10M product phase appears in the concentration region near the Ni_2AlMn composition. In the present study, the crystal structures of the martensite phase formed in the as-quenched and aged specimens of Ni–20, 21 and 22 at%Al–25 at%Mn alloys were examined by selected area electron diffraction (SAD) technique. The typical SAD patterns obtained from the 21 and 22 at%Al alloys are shown in Figs. 6 and 7. In the specimens quenched from 1000°C the major structures most frequently observed are the 2M, 14M and the 10M in the 20%Al, 21%Al and 22%Al alloys, respectively, along with small amounts of other minor structures besides these major phases. This result is in good agreement with the previous result.[2,14]

In the 21%Al and 22%Al specimens aged after quenching on the other hand, two new stacking sequences denoted as the 8M and the 10M′ structures respectively and shown in Figs. 6(b) and 7(b) were found. One typical characteristic feature of the 8M structure is the presence of $x/8\{220\}_{L2_1}$ reflections which suggest that this structure has a stacking periodicity eight times that of the $\{220\}_{L2_1}$ lattice planes. The conclusion from the crystallographic analysis of the SAD pattern from several directions is that the 8M structure has the $(5\bar{3})$ stacking sequence, as illustrated in Fig. 8. The 10M′ structure appearing in the as-aged 22%Al specimen is different from the 10M structure and has the following characteristic features;

(i) There are extra spots near $x/5\{220\}_{L2_1}$ reflections similar to those of the 10M structure, but the position of every extra spot is located at about $0.186 \cdot x\{220\}_{L2_1}$ which deviates from the precise $0.2 \cdot x\{220\}_{L2_1}$ position.

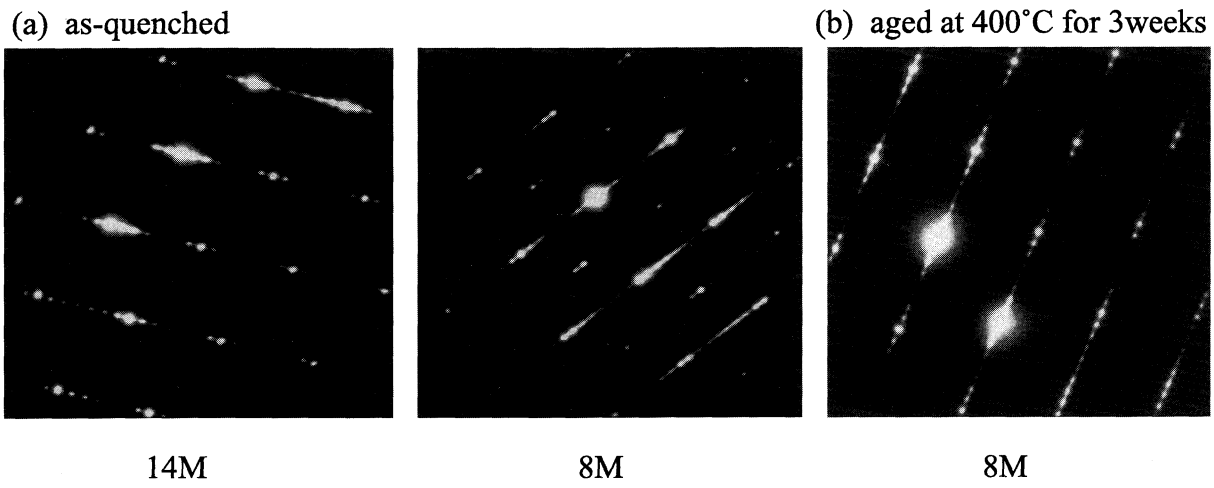

Fig. 6 The SADPs at 20°C taken from the martensite phases in the (a) as-quenched and (b) the aged Ni–21Al–25Mn specimens.

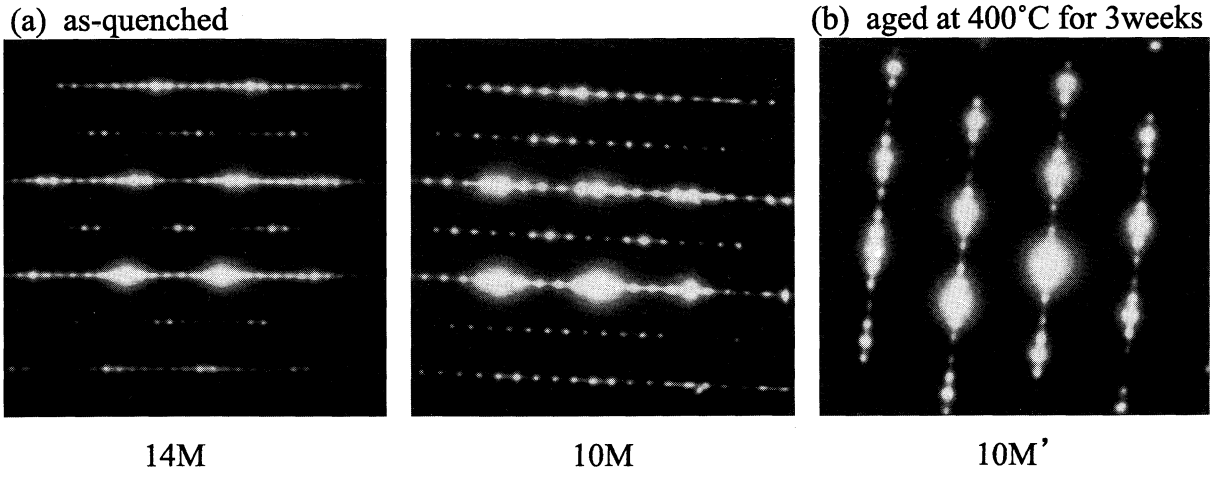

Fig. 7 The SADPs at −196°C taken from the martensite phases in the (a) as-quenched and (b) the aged Ni–22Al–25Mn specimens.

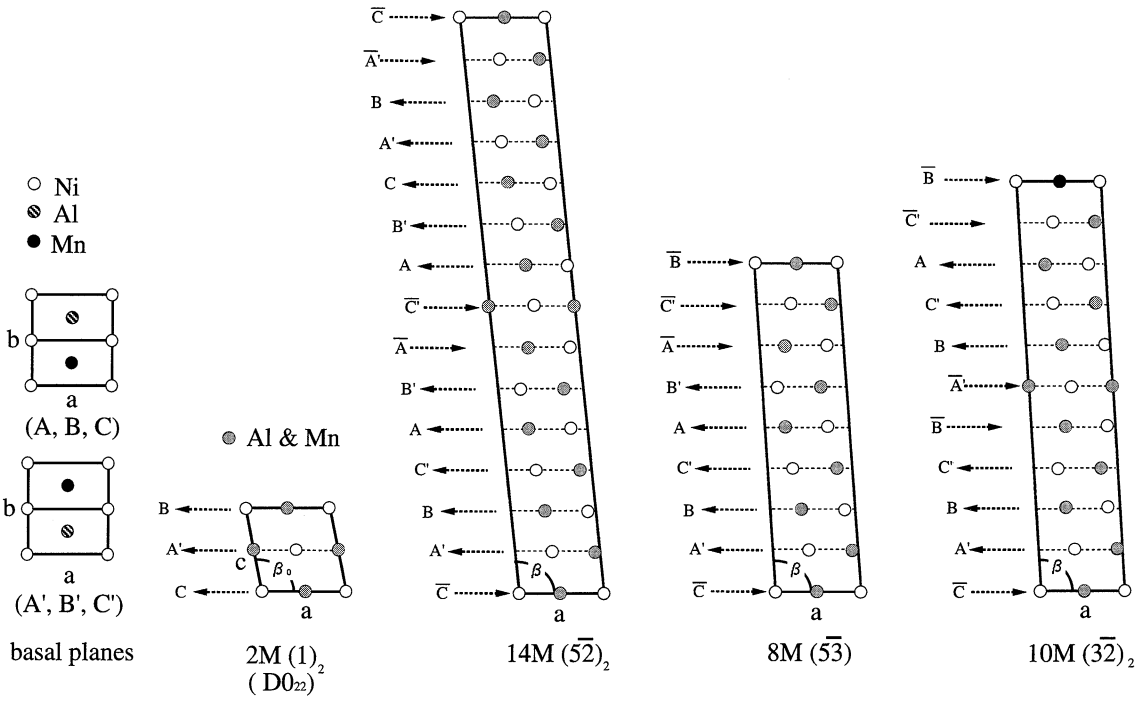

Fig. 8 Crystal structures of the 2M, 14M, 8M and 10M martensite phases martensitically formed from the $L2_1$ parent phase.

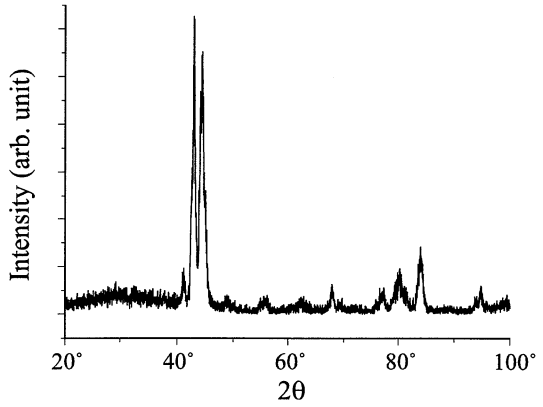

Fig. 9 The XRD powder pattern at −196°C taken of the martensite phase in the Ni–22Al–25Mn specimen aged at 400°C for 162 h.

(ii) The monoclinic symmetry of the 10M′ structure is the same as that of the 10M structure. However, while the monoclinic angle β of the 10M phase increases from about 90.5° up to about 91.5° with decreasing temperature from the *Ms* (=6°C) to −196°C, the 10M′ phase shows very small temperature dependence on the β angle which is in the range 90.5° and 91.0°, as shown in the SAD pattern (Fig. 7(b)).

Figure 9 shows the XRD powder pattern of the aged 22%Al alloy taken at −196°C. The diffraction pattern is very similar to that of the martensite phase in the Ni_2GaMn alloys reported as the orthorhombic ($Fmmm$) by Webster *et al.*[15] or as the tetragonal structure (I_4/mmm) structure by Wedel *et al.*,[16] and is comparable to the 10M′ structure deduced from the SAD pattern in the present work. Even though the crystal structure details of the 10M′ phase are as yet unknown, it has been confirmed by *in-situ* TEM observation that the 10M′ structure is no pre-martensite phase and that it exists in a wide temperature region below $Ms = -28$°C.

The results of the martensite structure determinations by the SAD technique are summarized in Table 4. It is seen that the most stable structure associated with increasing Al content from 20 to 22 at% changes in the order 2M-14M-8M-10M-10M′. It is also interesting to note that such the change of stacking structure is strongly related to the monoclinic angle β of each of these structures. By assuming that the $\{220\}_{L2_1}$ stacking unit in every martensite structure is the same as that in the 2M($D0_{22}$) structure, the monoclinic angle β of a structure with the $(a\bar{b})_n$ stacking sequence can be evaluated as

$$\tan(\beta - 90°) = A \cdot \tan(\beta_0 - 90°), \qquad (2)$$

where $A = (a-b)/(a+b)$ is a parameter indicating the extent of deviation from 90° in the angle β and the β_0 the monoclinic angle of the 2M or $D0_{22}$ unit. Assuming the $\beta_0 = 100°$, since the A values for the different stacking sequences are given as $A_{2M} = 1$, $A_{14M} = 0.43$, $A_{8M} = 0.25$ and $A_{10M} = 0.2$ from their stacking orders, the monoclinic angles of their structures can be estimated as $\beta_{2M} = 100°$, $\beta_{14M} = 94.32°$, $\beta_{8M} = 92.52°$ and $\beta_{10M} = 92.02°$ which are comparable to the experimental results from the electron diffraction study, $\beta_{14M} = 94.5°$ (as-quenched 22 at%Al alloy), $\beta_{8M} = 93.0°$ (as-aged 21 at%Al alloy) and $\beta_{10M} = 91.5°$ (as-quenched

Table 4 Crystal structure of the martensite phase in as-quenched and as-aged specimens.

Composition		Observed temp. (°C)	As-quenched	As-aged
at%Al	at%Mn			
20	25	20	2M(+14M)	2M
21	25	20	14M(+8M)	8M
22	25	−196	10M(+14M)	10M′

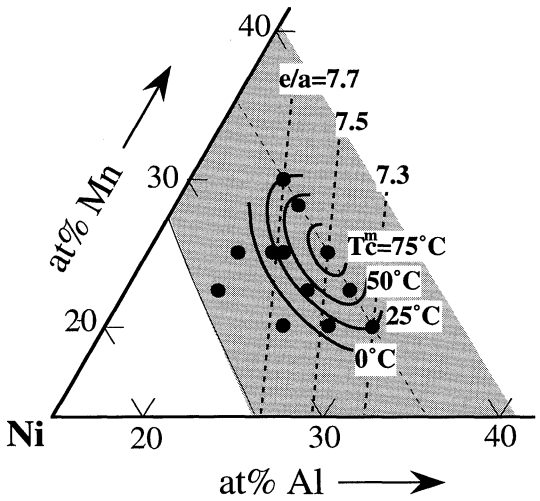

Fig. 10 The iso-T_c^m contours.

22 at%Al alloy). This result means that the monoclinic angle of the martensite phases gradually decreases in the order 2M-14M-8M-10M-10M′ with increasing Al content. More detailed studies are required to clarify the influence of the magnetic transition on the crystal structure of martensite phase and the role of ordering of the parent phase during aging in inducing the change from the 8M to the 10M′ structure.

3.3 Magnetic transition temperature

The Curie temperatures of the aged specimens were determined by DSC measurements. All the Curie temperature T_c^m data are listed in Table 1 and plotted in Fig. 2. The iso-T_c^m contours are also shown in Fig. 10. The Curie temperature has a maximum value of 91°C at the Ni_2AlMn stoichiometric composition, which drastically decreases on deviating from the stoichiometric composition, especially towards the Ni rich direction. The reasons for such Curie temperature behavior are not yet clear. Chernenko has reported that, in the Ni–Mn–Ga system the T_c^m and *Ms* temperatures can be normalized as a function of electron concentration e/a, assuming the following electron numbers per atom: Ni = 10, Mn = 7 and Ga = 3.[17] In our previous paper,[6] it was proposed that the same type of normalization on the basis of e/a for T_c^m and Ms_a could be extended to the Ni–Mn–Al system as well. Such a normalisation was applicable only to the *Ms* temperatures of alloys in the restricted region near the Ni_2AlMn stoichiometric composition as shown in Fig. 5(a), and not to the Curie temperatures shown in Figs. 2(c) and 10.

It has been reported in our previous paper[6] that the martensitic transformation in the Ni–Al–Mn ferromagnetic alloys influences the magnetic properties. The Ni–Al–Mn alloys show the same basic characteristic features as the Ni–Ga–Mn alloys and are potential candidates for use as new type of SM materials that can be controlled by an applied magnetic field. Further investigations on the magnetic and shape memory properties of these alloys in an applied extrinsic magnetic field will be reported in future articles.

4. Conclusions

(1) The B2/$L2_1$ ordering temperatures of the β single-phase alloys were determined by DSC measurements. A theoretical thermodynamic calculation of the ordering temperatures were made using the BWG approximation and the 1st and 2nd nearest neighbors interchange energies of each atomic pair in the Ni–Al–Mn system and the results compared.

(2) The *Ms* temperatures of the as-quenched and aged specimens were determined. The *Ms* temperature decreases when the parent phase orders to the $L2_1$ structure on low-temperature aging, and the difference in *Ms* between the as-quenched and the aged specimens is strongly related to the B2/$L2_1$ ordering temperatures.

(3) The crystal structures of martensite phases in the Ni–20 to 22 at%Al–25Mn alloys were determined by the selected area electron diffraction technique. Two new types of martensite structures, the 8M and the 10M′ structures were detected in the aged 21%Al and 22%Al specimens, respectively.

(4) The Curie temperatures of the aged alloys determined by DSC have a maximum at the Ni_2AlMn stoichiometric content and drastically decrease on deviating from the stoichiometric content, especially towards the Ni-rich directions.

Acknowledgements

The authors wish to thank Dr. L. Chandrasekaran of DERA, Farnborough, UK for useful comments, reading and helping in the presentation of the manuscript for publication. This work was supported by the Grant-in-Aids for Scientific Research from the Ministry of Education, Science, Sports and Culture, Japan. The authors also acknowledge the support from the Toray Science Foundation.

REFERENCES

1) R. Kainuma, M. Ise, K. Ishikawa, I. Ohnuma and K. Ishida: J. Alloys & Comp., **269** (1998), 173–180.
2) R. Kainuma, E. Nakano and K. Ishida: Metall. Mater. Trans. A, **27A** (1996), 4153–4162.
3) R. Kainuma, E. Nakano, K. Oikawa, K. Ishida and T. Nishizawa: Mat. Res. Soc. Symp. Proc., **246** (1992), 403–408.
4) S. Morito, T. Kakeshita, K. Hirata and K. Otsuka: Acta Mater., **46** (1998), 5377–5384.
5) Y. Sutou, I. Ohnuma, R. Kainuma and K. Ishida: Metall. Mater. Trans. A, **29A** (1998), 2225–2227.
6) F. Gejima, Y. Sutou, R. Kainuma and K. Ishida: Metall. Mater. Trans. A, **30A** (1999), 2721–2723.
7) K. Ullakko, J. K. Huang, V. V. Kokorin and R. C. O'Handley: Scripta Mater., **36** (1997), 1133–1138.
8) T. Maki: *Shape Memory Materials*, Ed. By K. Otsuka and C. M. Wayman, Cambridge Univ. press, (1998), pp. 117–132.
9) G. Inden: Acta Metall., **22** (1974), 945–951.
10) G. Inden: Z. Metallkde, **66** (1975), 577–582.
11) X. J. Liu, I. Ohnuma, R. Kainuma and K. Ishida: J. Phase Equilibria, **20** (1999), 45–56.
12) K. Ishikawa, M. Ise, I. Ohnuma, R. Kainuma and K. Ishida: Ber. Bunsenges. Phys. Chem., **102** (1998), 1206–1210.
13) S. M. Hao, K. Ishida and T. Nishizawa: Metall. Trans. A, **15A** (1984), 1819–1825.
14) S. Morito and K. Otsuka: Mater. Sci. Eng. A, **A208** (1996), 47–55.
15) P. J. Webster, K. R. A. Ziebeck, S. L. Town and M. S. Peak: Philis. Mag. B, **49** (1984), 295–310.
16) B. Wedel, M. Suzuki, Y. Murakami, T. Suzuki, D. Sindo and K. Itagaki: J. Alloys & Comp., **290** (1999), 137–143.
17) V. A. Chernenko: Scripta Mater., **40** (1999), 523–527.